

# Stabilization and rovibronic spectra of the *T*-shaped and linear ground-state conformers of a weakly bound rare-gas–homonuclear dihalogen complex: $\text{He}\cdots\text{Br}_2$

David S. Boucher, David B. Strasfeld, and Richard A. Loomis<sup>a)</sup>  
*Department of Chemistry, Washington University in St. Louis, One Brookings Drive, CB 1134,  
 Saint Louis, Missouri, 63130*

John M. Herbert  
*Department of Chemistry, University of California, Berkeley, California 94720*

Sara E. Ray and Anne B. McCoy<sup>b)</sup>  
*Department of Chemistry, The Ohio State University, Columbus, Ohio, 43210*

(Received 8 June 2005; accepted 30 June 2005; published online 14 September 2005)

Laser-induced fluorescence spectra of  $\text{Br}_2$  entrained in a He supersonic expansion have been recorded in the  $\text{Br}_2$  *B*-*X*, 8-0, 12-0, and 21-0 spectral regions at varying downstream distances, and thus different temperature regimes. Features associated with transitions of the *T*-shaped and linear  $\text{He}\cdots\text{Br}_2(X, \nu''=0)$  complexes are identified. The changes in the relative intensities of the *T*-shaped and linear features with cooling in the expansion indicate that the linear conformer is energetically more stable than the *T*-shaped conformer. A  $\text{He}+\text{Br}_2(X, \nu''=0)$  *ab initio* potential-energy surface, computed at the coupled cluster level of theory with a large, flexible basis set, is used to calculate the binding energies of the two conformers, 15.8 and 16.5  $\text{cm}^{-1}$  for the *T*-shaped and linear complexes, respectively. This potential and an excited-state potential [M. P. de Lara-Castells, A. A. Buchachenko, G. Delgado-Barrio, and P. Villareal, *J. Chem. Phys.* **120**, 2182 (2004)] are used to calculate the excitation spectra of  $\text{He}\cdots^{79}\text{Br}_2(X, \nu''=0)$  in the  $\text{Br}_2$  *B*-*X*, 12-0 region. The calculated spectra are used to make spectral assignments and to determine the energies of the excited-state intermolecular vibrational levels accessed in the observed transitions. Temperature-dependent laser-induced fluorescence spectra and a simple thermodynamic model [D. S. Boucher, J. P. Darr, M. D. Bradke, R. A. Loomis, and A. B. McCoy, *Phys. Chem. Chem. Phys.* **6**, 5275 (2004)] are used to estimate that the linear conformer is 0.4(2)  $\text{cm}^{-1}$  more strongly bound than the *T*-shaped conformer. Two-laser action spectroscopy experiments reveal that the binding energy of the linear  $\text{He}\cdots^{79}\text{Br}_2(X, \nu''=0)$  conformer is 17.0(8)  $\text{cm}^{-1}$ , and that of the *T*-shaped  $\text{He}\cdots^{79}\text{Br}_2(X, \nu''=0)$  conformer is then 16.6(8)  $\text{cm}^{-1}$ , in good agreement with the calculated values. © 2005 American Institute of Physics. [DOI: 10.1063/1.2006675]

## I. INTRODUCTION

The rare-gas–dihalogen van der Waals complexes have proven to be ideal systems for studying the nature of long-range intermolecular forces, photodissociation dynamics, and energy redistribution mechanisms.<sup>1,2</sup> Members of this class of weakly bound complexes exhibit dynamics and spectra that are complicated enough to make them interesting, yet their structural simplicity makes them amenable to detailed theoretical investigation. The confluence of theory and experiment has been successful and has enabled advancing theoretical methods to be tested. High-level *ab initio* treatments of the rare-gas–dihalogen ground-state intermolecular potential-energy surfaces (PESs) indicate the existence of minima in the *T*-shaped and linear configurations, with the global minimum being in the linear configuration.<sup>3</sup> The rovibronic spectra of these complexes, recorded using mostly laser-induced fluorescence (LIF) and two-color action spec-

troscopy in the  $B^3\Pi_{0+} \leftarrow X^1\Sigma^+$  electronic region of the dihalogen, however, most often contain discrete features associated with transitions of a rigid *T*-shaped geometry in both the ground and excited states.<sup>2</sup> Spectroscopic evidence supporting the existence of linear isomers has been rather limited; restricted predominantly to microwave studies.<sup>4–7</sup> As a consequence, the interactions and dynamics in the *T*-shaped regions of ground- and excited-state potentials have been comprehensively interrogated, often as a function of dihalogen vibrational excitation in the excited state. In contrast, little experimental information associated with the other regions of the multidimensional intermolecular ground- and excited-state PESs have been revealed.

Recently, we reported that discrete features associated with transitions of  $\text{He}\cdots\text{ICl}(X, \nu''=0)$  complexes with rigid *T*-shaped and linear geometries are observable in LIF and action spectra recorded in the  $\text{ICl}$  *B*-*X*,  $\nu'-0$  spectral region.<sup>8,9</sup> High-level *ab initio* calculations revealed that the ground-state  $\text{He}+\text{ICl}(X, \nu''=0)$  intermolecular PES possesses minima in the linear  $\text{He}-\text{I}-\text{Cl}$ , near *T*-shaped, and antilinear

<sup>a)</sup>Electronic mail: loomis@wustl.edu

<sup>b)</sup>Electronic mail: mccoy@chemistry.ohio-state.edu

I–Cl–He orientations with the global minimum being in the linear configuration.<sup>10</sup> The lowest-energy intermolecular vibrational level is localized in the linear well, and the next lowest intermolecular vibrational level is in the *T*-shaped well. Subsequent calculations found that there is an effective barrier of  $\sim 11$   $\text{cm}^{-1}$  between the *T*-shaped and linear levels, and the corresponding probability amplitudes have  $>99.99\%$  of their amplitude in a single well.<sup>9</sup> Consequently, complexes stabilized in these two different intermolecular vibrational levels can be considered to be distinct linear and *T*-shaped conformers of the  $\text{He}\cdots\text{ICl}(X, \nu''=0)$  complex.

We also undertook investigations focusing on how these  $\text{He}\cdots\text{I}^{35}\text{Cl}(X, \nu''=0)$  conformers are preferentially stabilized within a free-jet expansion.<sup>11</sup> Using a simple thermodynamic model, the rotational temperature dependence of the ratios of the peak intensities of the *T*-shaped and linear LIF features was used to estimate the difference in the binding energies of the linear and *T*-shaped intermolecular vibrational levels.<sup>12</sup> It was found that the linear  $\text{He}\cdots\text{I}^{35}\text{Cl}(X, \nu''=0)$  conformer is  $\sim 2.5$   $\text{cm}^{-1}$  more strongly bound than the *T*-shaped complex. Furthermore, action spectroscopy was used to directly obtain a binding energy of  $22.0(2)$   $\text{cm}^{-1}$  for the linear  $\text{He}\cdots\text{I}^{35}\text{Cl}(X, \nu''=0)$  conformer.<sup>12</sup> The binding energy of the *T*-shaped conformer was then estimated to be  $19.5(6)$   $\text{cm}^{-1}$ . The difference in the binding energies is similar to that calculated,  $\sim 3$   $\text{cm}^{-1}$ , with the linear and *T*-shaped  $\text{He}\cdots\text{I}^{35}\text{Cl}(X, \nu''=0)$  conformers predicted to be bound by  $18.26$  and  $15.14$   $\text{cm}^{-1}$ , respectively.<sup>10</sup> Using the experimental binding energy of the ground-state *T*-shaped conformer and the wave-number shift of the *T*-shaped band origin from the monomer band origin in the ICl *B*-*X*, 2-0 and 3-0 regions, excited-state binding energies of  $16.3(6)$  and  $16.2(6)$   $\text{cm}^{-1}$  were determined for the  $\text{He}+\text{I}^{35}\text{Cl}(B, \nu'=2)$  and  $\text{He}+\text{I}^{35}\text{Cl}(B, \nu'=3)$  intermolecular potentials, respectively.<sup>12</sup> A detailed comparison of the experimental and theoretical spectra permitted spectral assignments to be made and allowed the energies of the  $n'=0-6$  bound  $\text{He}\cdots\text{I}^{35}\text{Cl}(B, \nu'=3)$  intermolecular levels to be determined. A particularly significant result from these studies is that the  $\text{He}+\text{ICl}(B^3\Pi_{0u+}, \nu')$  intermolecular potential is not purely repulsive along the He–ICl dissociation coordinate when the complex is in the collinear He–I–Cl geometry. Instead, bound intermolecular levels sample this angular region of the potential.

The  $\text{He}\cdots\text{ICl}$  experiments revealed unprecedented information regarding the ground- and excited-state potentials of a rare-gas–dihalogen complex. In order to further investigate the intermolecular interactions within such systems, we sought to carry out similar investigations on a complex containing a rare-gas atom and a homonuclear diatomic molecule,  $\text{Br}_2$ , to determine what role, if any, the symmetry of the molecule has on the intermolecular interactions. The rovibronic spectrum of  $\text{He}\cdots^{79}\text{Br}_2$  has been recorded in the  $\text{Br}_2$  *B*-*X*, 8-0 region using action spectroscopy,<sup>13</sup> and has proved to be a valuable guide in the efforts presented here. The spectrum contains two distinct features at transition energies to just higher wave-numbers than the monomer band.<sup>13</sup> One feature, shifted by  $\sim 4$   $\text{cm}^{-1}$  from the  $\text{Br}_2$  band origin, is attributed to transitions from a rigid *T*-shaped

$\text{He}\cdots^{79}\text{Br}_2(X, \nu''=0)$  complex to a  $\text{He}\cdots^{79}\text{Br}_2(B, \nu'=8)$  excited-state intermolecular vibrational level that also has a rigid *T*-shaped geometry. A weaker band was observed  $\sim 9$   $\text{cm}^{-1}$  to higher energy than the monomer band origin. Initial simulations of this feature were not successful, and it was speculated that this feature could be associated with transitions of the ground-state *T*-shaped complex to an excited-state level with intermolecular bending excitation.<sup>13</sup> Theoretical efforts aimed at accurately predicting the rovibronic spectrum of the  $\text{He}\cdots^{79}\text{Br}_2$  complex indicate that there are two distinct conformers in the ground state, one with a *T*-shaped geometry and another with a linear structure. Subsequent calculations have predicted the binding energies of the conformers to be  $17.7$  and  $17.2$   $\text{cm}^{-1}$  for the *T*-shaped and linear complexes, respectively.<sup>14</sup> Even more recently, calculations have predicted the linear complex to be slightly more strongly bound than the *T*-shaped species with binding energies of  $14.90$  and  $16.02$   $\text{cm}^{-1}$  for the *T*-shaped and linear complexes.<sup>15</sup> The results of both of these calculations indicate that the two conformers are nearly isoenergetic and may be stabilized in the experiments performed in supersonic expansions. Furthermore, the calculations suggest that the higher-energy excitation feature in the  $\text{He}\cdots^{79}\text{Br}_2$  spectrum is mostly comprised of rovibrational lines associated with transitions of the linear  $\text{He}\cdots^{79}\text{Br}_2(X, \nu''=0)$  complex to levels with bending excitation in the electronically excited-state potential.<sup>14,16</sup> A small admixture of weaker lines in this feature that are associated with transitions of the *T*-shaped conformer is also observed in the calculated spectrum.

The previous  $\text{He}\cdots^{79}\text{Br}_2$  results<sup>13,14,16</sup> suggest that similar experiments to those performed on the  $\text{He}\cdots\text{ICl}$  system<sup>9,11,12</sup> could provide quantitative information concerning the energetics of the *T*-shaped and linear  $\text{He}\cdots^{79}\text{Br}_2(X, \nu''=0)$  conformers. Furthermore, detailed comparisons of the experimental data with high-level theoretical results should reveal many of the properties of the multidimensional intermolecular potentials in the ground and excited states. For this reason, we have chosen to record  $\text{He}\cdots\text{Br}_2$  spectra under varying expansion conditions, to measure the binding energies of the ground- and excited-state complexes, and to perform additional calculations to gain insights into intermolecular interactions and the role that the symmetry of the molecules has on these rare-gas–dihalogen interactions. Preliminary calculations of the bound-state energies of  $\text{He}\cdots\text{Br}_2(X, \nu''=0)$ , using the potential surface calculated by Prosmi *et al.*,<sup>17</sup> indicated that the sampling of the angular dependence was not sufficient to obtain quantitative results. Therefore, we elected to recalculate this surface at the CCSD(T) level of theory (i.e., coupled-cluster singles, doubles, and noniterative triples) at increments of  $10^\circ$ . For the excited-electronic state we find that a diatomic in molecule (DIM) potential based on the  $\text{He}\cdots\text{Br}$  potentials reported in Ref. 18 provides an accurate representation of the potential. Using these potentials and the assumption that the transition moment lies along the Br–Br bond, we are able to obtain temperature-dependent spectra for  $\text{He}\cdots\text{Br}_2$  that are in quantitative agreement with what is seen experimentally.

## II. EXPERIMENT

Ground-state He...Br<sub>2</sub>(*X*, *v*'=0) complexes were stabilized in a pulsed supersonic expansion. A He carrier gas with a backing pressure *P*<sub>0</sub> of 28.6 bar was passed through a sample cell containing liquid bromine. The vessel was maintained at a temperature of -15 °C, at which the bromine vapor pressure is ~0.03 bar. The resulting He/Br<sub>2</sub> mixture, with a bromine concentration of ~1000 ppm, was expanded at 10 Hz from a pulsed valve with a nozzle diameter *d* of 1.0 mm into a chamber maintained at a pressure below 20 mTorr by a root blower pumping system with a speed of 1900 l/s.

LIF spectra were recorded in the Br<sub>2</sub> *B*-*X*, 8-0, 12-0, and 21-0 spectral regions using a commercial Nd:YAG (yttrium aluminum garnet) pumped dye laser with a resolution of 0.06 cm<sup>-1</sup>. The laser beam was spatially filtered to a diameter of ~3 mm at varying downstream distances *x* within the supersonic expansion. Neutral density filters were used to attenuate the laser pulse energies to ~75 μJ and 1.1 mJ when scanning over the monomer and complex features, respectively. Resultant Br<sub>2</sub> *B*→*X*, *v*'→*v*' fluorescence was collected and imaged onto a visible wavelength photomultiplier tube using an F/1 mirror and telescope assembly. A 10×4-mm<sup>2</sup> mask was positioned within the assembly with the long axis oriented parallel to the axis of the expansion so that only fluorescence from the centermost region of the expansion was collected. A boxcar integrator was used to record the intensity of the LIF as a function of wavelength.

Since there are intense <sup>81,81</sup>Br<sub>2</sub>, <sup>79,81</sup>Br<sub>2</sub>, and <sup>79,79</sup>Br<sub>2</sub> monomer features as well as multiple weaker He...<sup>81,81</sup>Br<sub>2</sub>, He...<sup>79,81</sup>Br<sub>2</sub>, and He...<sup>79,79</sup>Br<sub>2</sub> features throughout the Br<sub>2</sub> *B*-*X* region that may to some extent overlap neighboring transitions, action spectra of the He...<sup>79,81</sup>Br<sub>2</sub> and He...<sup>79,79</sup>Br<sub>2</sub> complexes were recorded in the Br<sub>2</sub> *B*-*X*, 12-0 spectral region at multiple downstream distances. These action spectra were acquired by scanning an excitation laser through the 12-0 region and monitoring the fluorescence induced by a second laser fixed in wavelength on the band heads of either the <sup>79,81</sup>Br<sub>2</sub> or <sup>79,79</sup>Br<sub>2</sub> *E*-*B*, 1-11 transitions. By probing the vibrational predissociation product channel for a specific isotopomer, excitation spectra comprised only of that He...Br<sub>2</sub> isotopomer are acquired.<sup>13,19</sup> The excitation laser was the same as that used in the LIF experiments, and the doubled output of a second dye laser with a resolution of 0.06 cm<sup>-1</sup> was used as the probe laser. The pump and probe laser beams were spatially overlapped using a dichroic mirror with the pump pulse preceding the probe pulse by 15 ns. Neutral density filters were used to reduce the pump energies to ~1 mJ, and it was empirically determined that pulse energies ≤30 μJ/pulse were required to avoid saturating the probe transitions. A 15-nm narrow bandpass filter centered at 267 nm was placed in front of an ultraviolet-enhanced photomultiplier tube to detect Br<sub>2</sub> *E*→*X*, 1→*v*' emission and block laser scatter and Br<sub>2</sub> *B*→*X* fluorescence.

Action spectroscopy was also used in a similar manner as reported previously<sup>9,20-22</sup> to investigate the bound-free transitions of the He...<sup>79,79</sup>Br<sub>2</sub>(*X*, *v*'=0) complexes to the continuum of states lying above the He+<sup>79</sup>Br<sub>2</sub>(*B*, *v*'=11) in-

termolecular asymptote. For these experiments, the probe laser was fixed on the *R*-band head of the <sup>79</sup>Br<sub>2</sub> *E*-*B*, 1-11 transition and the excitation laser was scanned through the <sup>79</sup>Br<sub>2</sub> *B*-*X*, 11-0 spectral region.

## III. THEORY

### A. He+Br<sub>2</sub> potential-energy surfaces

Counterpoise-corrected intermolecular potential energies for He...Br<sub>2</sub>(*X*, *v*'=0) were calculated at the CCSD(T) level for a fixed Br-Br distance at the equilibrium value, 2.28 Å, using GAUSSIAN 98.<sup>23</sup> Core electrons for Br (including the 3*d* shell) were replaced by the Stuttgart/Dresden (SDD) pseudopotential,<sup>24</sup> and valence electrons were represented using the complementary SDD basis of *s* and *p* functions augmented with Pople's *sp* diffuse functions and 3*df* polarization functions, for an overall valence Br basis of SDD + *G*(3*df*). Dunning's aug-cc-pVQZ basis was used for He. To this atom-centered He...Br<sub>2</sub> basis was added a (3*s* 3*p* 2*d* 2*f* 1*g*) set of uncontracted bond functions centered at the midpoint between He and the Br<sub>2</sub> center of mass, with exponents taken from Ref. 25. Six Cartesian *d* functions and ten *f* functions were used in all cases, for a total of 200 basis functions.

The He+Br<sub>2</sub>(*X*, *v*'=0) intermolecular potential is evaluated in terms of the two Jacobi coordinates for an atom-diatom system; the distance between the helium atom and the center of mass of the Br-Br bond is represented by *R*, while *θ* is the angle between *R* and the Br-Br bond axis, and the Br-Br internuclear distance is *r*. A two-dimensional potential function *V*(*R*, *θ*) was constructed as an expansion in direct-product basis functions

$$f_{kl}(R, \theta) = F_k(R)P_l(\cos \theta), \quad (1)$$

where *P*<sub>*l*</sub> denotes a Legendre polynomial. Radial basis functions *F*<sub>*k*</sub>(*R*), *i* ∈ {1, 2, ..., *N*<sub>*θ*</sub>} were constructed by one-dimensional least-squares fits of the potential energies at each incremental value of *θ*. For the radial basis functions *F*<sub>*k*</sub>(*R*), a Morse function plus dispersion terms was utilized,

$$F_k(R) = V(R, \theta_k) = D_k e^{-\alpha_k(R-R_{p,k})} [e^{-\alpha_k(R-R_{p,k})} - 2] - \sum_{n=2}^6 \frac{C_{2n,k}}{R^{2n}}. \quad (2)$$

The dispersion terms in addition to the *R*<sup>-6</sup> and *R*<sup>-12</sup> dependences were necessary in order to achieve sub-cm<sup>-1</sup> accuracy in the fit. It should be noted that due to the addition of these dispersion terms, one cannot equate *D*<sub>*k*</sub> to the dissociation energy or *R*<sub>*p,k*</sub> to the value of *R* where the potential is minimized.

For the present study, we use two representations of the He+Br<sub>2</sub>(*B*, *v*') electronically excited-state potential described in Ref. 18. Specifically, we fit the reported *ab initio* points in the same manner as described above for the *X*-state surface. A DIM surface that is based on spline interpolations of the two radial cuts, reported in Table III of Ref. 18, was also utilized. In order to obtain an intermolecular potential from the DIM surface, the energies of a specific vibrational level of Br<sub>2</sub> are calculated as a function of *R* and *θ*. These

points are used to provide an adiabatic potential from which we can investigate the intermolecular interactions.

## B. He $\cdots$ Br<sub>2</sub> rovibronic spectra

The methods used to obtain the rovibrational spectra, transition frequencies and intensities, are described in detail elsewhere.<sup>9</sup> Briefly, the intermolecular vibrational Hamiltonian is given by

$$\hat{H} = \frac{b_v}{\hbar^2} |J-l|^2 + \frac{l^2}{2\mu_R R^2} - \frac{\hbar^2}{2\mu_R} \frac{\partial^2}{\partial R^2} + V(R, \theta). \quad (3)$$

The Schrödinger equation is solved for each value of  $K$  using a discrete variable representation (DVR) for  $R$  and  $\theta$ . A grid of 60 evenly spaced points in  $R$ , ranging from 2 to 10 Å, is used for these calculations while the angular grid is obtained

using 30 DVR points based on the associated Legendre polynomials. Once the wave functions and energies have been obtained for each value of  $K$ , the lowest 20 states are retained and used to set up the full Hamiltonian matrix, including the Coriolis coupling terms. As the rotational temperatures probed in the experiment are less than 1 K, only the states with  $J < 9$  are evaluated. As in our previous work,<sup>9</sup> we embed our body-fixed  $z$  axis along the Br–Br bond,  $r$ .

Once the energies and wave functions have been evaluated, we obtain the intensities in the same manner as described previously.<sup>9</sup> The only change is that we introduce the nuclear spin weightings for Br<sub>2</sub>, three for states with even parity, five for states with odd parity. It should be noted that there was a typographical error in Eq. (12) of Ref. 9. As such, the expression for the intensities is given by

$$I_{n_X, J_X, \pi_X; n_B, J_B, \pi_B} \propto g_{n_X, J_X, \pi_X} e^{-E_{n_X, \pi_X}^{J_X, \pi_X} / k_B T} G(J_X, J_B - J_X) \times \left| \sum_{i,j,K} (d_{i,j,K}^{n_B, \pi_B, J_B, M_B})^* c_{i,j,K}^{n_X, \pi_X, J_X, M_X} O(J_X, J_B - J_X, K) \delta_{\pi_X + \pi_B, 0} \right|^2, \quad (4)$$

where  $c$  and  $d$  represent the coefficients in the expansion of the wave functions on the  $X$  and  $B$  electronic states, respectively. The nuclear spin weighting,  $g_n$ , is dependent on  $n$ , the state number for a given value of the total angular momentum  $J$  and parity  $\pi$ . Following standard notation

$$\begin{aligned} G(J, -1) &= \frac{1}{J}, \\ G(J, 0) &= \frac{2J+1}{J(J+1)}, \\ G(J, +1) &= \frac{1}{J+1}, \end{aligned} \quad (5)$$

and

$$\begin{aligned} O(J, -1, K) &= -\sqrt{J^2 - K^2}, \\ O(J, 0, K) &= K, \\ O(J, +1, K) &= -\sqrt{(J+1)^2 - K^2}, \end{aligned} \quad (6)$$

The calculated stick spectra are convoluted with a Lorentzian line-shape function to facilitate comparison with the experimental spectra.

## IV. RESULTS

### A. Theoretical He+<sup>79</sup>Br<sub>2</sub>( $X, \nu''=0$ ) properties

Calculated He $\cdots$ Br<sub>2</sub> intermolecular potential energies are listed in Tables I and II. Compared to the He $\cdots$ Br<sub>2</sub>( $X, \nu''=0$ ) basis used by Valdés *et al.*<sup>15</sup> and Prosmiiti *et al.*,<sup>17</sup> we have reduced the He-centered basis from aug-cc-pV5Z to aug-cc-pVQZ, which reduces the total number of

basis functions by 50 with only a minor effect on the calculated interaction energies. The differences between our calculated intermolecular potential energies and those of Prosmiiti *et al.*<sup>17</sup> are not more than 0.7 cm<sup>-1</sup> for  $\theta=0^\circ$ , and not more than 2.5 cm<sup>-1</sup> for  $\theta=90^\circ$ . Comparisons of our values with those of Valdés *et al.*<sup>15</sup> indicate a slightly smaller discrepancy for the linear orientation, 0.6 cm<sup>-1</sup>, and the same 2.5-cm<sup>-1</sup> difference in the  $T$ -shaped orientation. The larger discrepancies at the  $T$ -shaped geometries reflect the somewhat greater angular flexibility afforded by He-centered  $g$  functions in the aug-cc-pV5Z basis.

The best-fit parameters from Eq. (2) that define the radial basis functions,  $D_k$ ,  $\alpha_k$ ,  $R_{p,k}$ , and  $C_{n,k}$ , are listed in Table III. Agreement to better than 0.02 cm<sup>-1</sup> versus the *ab initio* data points was achieved for each angle except at  $\theta=60^\circ$ , where the root-mean-square deviation in the radial fit was 0.1 cm<sup>-1</sup>. Given the high quality of the radial fit, we utilized the functions  $F_k(R) = V(R, \theta_k)$  to generate a large set of data points  $\{V(R_j, \theta_k)\}$  along these fixed- $\theta$  slices through the potential ( $\sim 100$  points per angle). The unknown expansion coefficients for  $V$  in the  $f_{kl}$  basis can then be expressed in terms of these points, and linear combination coefficients determined by singular value decomposition. Partial waves  $l = 0, 2, 4, \dots, 18$  afforded a two-dimensional potential  $V(R, \theta)$  that is essentially exact along the radial slices  $F_k(R)$ .

The fitted potential function  $V(R, \theta)$  is plotted in Fig. 1(a). The well depth for the linear complex is  $D_e'' = 49.45$  cm<sup>-1</sup> at an internuclear distance of  $R_e'' = 4.412$  Å. For the  $T$ -shaped complex the corresponding values are  $D_e'' = 40.64$  cm<sup>-1</sup> and  $R_e'' = 3.599$  Å. These values differ by  $< 0.7$  cm<sup>-1</sup> and  $< 0.02$  Å from those reported in Ref. 17 for both orientations. The agreement with the orientations at the minima reported in Ref. 15 is not as good with differences of  $< 0.8$  cm<sup>-1</sup> and  $< 0.02$  Å for the linear orientation, but nearly

TABLE I. Counterpoise-corrected intermolecular potential energies for He···Br<sub>2</sub>(X) at r(Br–Br)=2.28 Å. The numbers in parentheses indicate differences between the values of this work and those calculated in Ref. 15/Ref. 17.

<i>R</i> /Å <sup>a</sup>	$\Delta E/\text{cm}^{-1}$							
	$\theta=0^\circ$		$\theta=30^\circ$		$\theta=60^\circ$		$\theta=90^\circ$	
2.875	6.3							
3.000	-29.3	(0.3/0.3)					52.2	(2.5/2.5)
3.125	-44.9						3.7	
3.250	-49.4	(0.6 <sup>b</sup> /0.6)					-23.0	(2.1/2.1)
3.375	-48.1						-36.3	
3.500	-44.0	(0.6/0.6)			131.2		-41.3	(1.8/1.8)
3.625	-38.9						-41.6	
3.750	-33.6	(0.5/0.7)			25.6		-39.3	(1.3/1.7)
3.875	-28.7				1.4		-35.9	
4.000	-24.4	(0.5/0.4)	66.7		-11.2	(1.0/1.0)	-31.9	(1.0/1.0)
4.125					-17.9			
4.250	-17.4	(0.4/0.4)	-4.4	(0.7/0.7)	-20.5	(0.7/0.7)	-24.3	(0.8/0.7)
4.375			-17.6		-20.9			
4.500	-12.4	(0.3/0.3)	-23.5	(0.6/0.6)	-20.0	(0.6/0.6)	-18.0	(0.6/0.6)
4.625			-25.1		18.3			
4.750	-9.0		-24.5	(0.5/0.4)	-16.5		-13.3	
4.875			-22.7					
5.000	-6.6	(0.2/0.2)	-20.4	(0.4/0.3)	-12.8	(0.3/0.3)	-9.8	(0.4/0.3)
5.250			-15.7		-9.7			
5.500	-3.7		-11.7	(0.2/0.3)	-7.3	(0.2/0.2)	-5.4	
5.875			-7.5					
6.250	-1.7		-4.9		-3.2		-2.5	
7.000	-0.86	(0.0/0.0)	-2.2	(0.1/0.1)	-1.5	(0.0/0.2)	-1.2	(0.0/0.0)
9.000	-0.2	(0.0/0.0)	-0.4	(0.0/0.0)	-0.3	(0.0/0.0)	-0.3	(0.0/0.0)

<sup>a</sup>To conform with Refs. 15 and 17, *R* indicates the smaller He–Br distance when  $\theta=0^\circ$ , while for nonlinear complexes *R* is the distance from He to the Br<sub>2</sub> center of mass.

<sup>b</sup>We believe that the value of  $-48.11 \text{ cm}^{-1}$  for  $r=2.28 \text{ \AA}$  and  $R=3.25 \text{ \AA}$ , which is listed in Table I of Ref. 15, contains a typographical error and should have been listed as  $-48.81 \text{ cm}^{-1}$  and the reported difference is based on this value.

$9.3 \text{ cm}^{-1}$  and  $\sim 0.05 \text{ \AA}$  for the *T*-shaped orientation. We used our ground-state potential to obtain the rotation-vibration energies and wave functions for He···<sup>79</sup>Br<sub>2</sub>(X,  $\nu''=0$ ), as described above. While for the present study we are only going to be concerned with the three lowest intermolecular vibrational energy levels, we report the energies of all of the  $J''=0$  states that are bound by at least  $1 \text{ cm}^{-1}$  in Table IV. To illustrate the extent of localization and delocalization of the wave functions that correspond to the energies reported in Table IV, we have performed an adiabatic calculation and plotted the results in Fig. 2(a). Specifically, for each value of  $\theta$ , we solve the Schrödinger equation:

$$\left[ -\frac{\hbar^2}{2\mu_R} \frac{\partial^2}{\partial R^2} + V(R, \theta) \right] \phi(R; \theta) = V_n(\theta) \phi(R; \theta). \quad (7)$$

The lowest-energy  $\theta$ -dependent energy eigenvalues  $V_0(\theta)$  provide a one-dimensional adiabatic potential. Using this surface, along with the kinetic energy in  $\theta$ , we obtain the corresponding adiabatic energies and wave functions. The corresponding probability amplitudes are plotted on the same graph, shifted so that zero-probability amplitude corresponds to the adiabatic energy of the state. Because an adiabatic approximation was used to obtain the energies and wave functions, these energies will differ slightly from those reported in Table IV.

The plot indicates that the two lowest-energy intermolecular levels represent the symmetric and antisymmetric linear combinations of the two states that have the helium atom localized near one of the Br atoms along the Br–Br axis. The next lowest-energy level corresponds to the helium atom being localized in a *T*-shaped configuration, relative to the Br–Br bond. Although the energy difference between these levels is only  $0.65 \text{ cm}^{-1}$ , the three levels are well-localized in either the *T*-shaped or linear minima of the potential. As such, we refer to the two lowest-energy levels,  $n''=0$  and 1, which are both bound by  $16.46 \text{ cm}^{-1}$ , as the linear conformer of the He···Br<sub>2</sub>(X,  $\nu''=0$ ) complex and the  $n''=2$  level that is bound by  $15.81 \text{ cm}^{-1}$  as the *T*-shaped conformer. The remaining bound levels with  $J''=0$  are close to or above the barrier for free rotation of the helium around the Br<sub>2</sub> and, as such, have amplitudes in both the linear and *T*-shaped wells of the intermolecular PES. It is important to note that while the potential supports seven levels that are bound by at least  $1.0 \text{ cm}^{-1}$ , none of these levels contain vibrational excitation in the He–Br<sub>2</sub> stretching coordinate. This can be seen by small changes in  $\langle R \rangle$  and  $\sqrt{\langle R^2 \rangle - \langle R \rangle^2}$  in the third and fourth columns of Table IV as  $n''$  increases from zero to five. As the  $n''=6$  state is near the dissociation threshold this state begins

TABLE II. Counterpoise-corrected intermolecular potential energies for He $\cdots$ Br $_2$ (X) at r(Br-Br)=2.28 Å, for angles not considered in Refs. 15 and 17.

$R/\text{Å}^a$	$\Delta E/\text{cm}^{-1}$					
	$\theta=10^\circ$	$\theta=20^\circ$	$\theta=40^\circ$	$\theta=50^\circ$	$\theta=70^\circ$	$\theta=80^\circ$
3.125						58.0
3.250						12.4
3.375						-13.5
3.500					23.7	-27.0
3.625					-1.5	-32.8
3.750					-15.3	-34.2
3.875				44.2	-22.2	-32.9
4.000	30.7	60.8	44.2	12.9	-24.7	-30.4
4.125	-12.6	11.6	11.5	-4.9	-24.8	-27.4
4.250	-33.6	-14.6	-6.8	-14.4	-23.4	-24.2
4.375	-41.8	-27.1	-16.3	-18.8	-21.4	
4.500	-43.0	-31.8	-20.4	-20.1	-19.2	-18.4
4.625	-40.6	-32.2	-21.4	-19.7		
4.750	-36.6	-30.3	-20.7	-18.4	-14.8	-13.7
4.875	-32.2	-27.4	-19.2	-16.7		
5.000	-27.8	-24.2	-17.3	-14.9	-11.2	-10.1
5.250	-20.2	-18.1	-13.4	-11.4	-8.4	
5.500	-14.5	-13.3	-10.1	-8.6	-6.3	-5.6
5.875	-8.9	-8.3	-6.5		-4.1	
6.250	-5.7	-5.3	-4.3	-3.7	-2.8	-2.5
7.000	-2.5	-2.3	-2.0	-1.7	-1.4	-1.3
9.000	-0.4	-0.4	-0.4	-0.3	-0.3	-0.2

<sup>a</sup>To conform with Refs. 15 and 17,  $R$  indicates the smaller He-Br distance when  $\theta=0^\circ$ , while for nonlinear complexes  $R$  is the distance from He to the Br $_2$  center of mass.

to sample the long-range part of the potential, leading to an increase in the values of  $\langle R \rangle$  and  $\sqrt{\langle R^2 \rangle - \langle R \rangle^2}$  in spite of the fact that there is no node in  $R$ .

## B. Theoretical He+ $^{79}\text{Br}_2(B, \nu')$ properties

We use two representations of the He+Br $_2(B, \nu')$  excited-state intermolecular PES, described in Ref. 18: a PES obtained by fitting the *ab initio* points reported in that paper and a DIM PES based on a spline interpolation of the two radial cuts reported in Table III of Ref. 18, and plotted in Fig. 1(b). In order to obtain an intermolecular potential from the DIM surface, we calculate the energies of the  $\nu'=8, 12$ , or 21 levels of Br $_2(B, \nu')$  as a function of  $R$  and  $\theta$ . These provide adiabatic potentials from which we can investigate

the intermolecular interactions. The calculated energies of all of the bound intermolecular vibrational levels obtained from the DIM surface are reported in Table V. For comparison, the energies of the levels calculated using the He+Br $_2(B, \nu'=12)$  *ab initio* PES are included, as are the experimental energies of the bound levels, determined as described in the following section. The probability amplitudes of the bound He $\cdots^{79}\text{Br}_2$  intermolecular levels, obtained from the DIM surface, are superimposed on the angular adiabatic potential in Fig. 2(b). Here, only the  $n'=0$  and 1 levels are localized in the T-shaped minimum of the potential. All other states have sufficient energy to sample all angles, and, as a result will be referred to as hindered rotor levels in the discussion that follows. The probability amplitudes obtained from the *ab initio* surface are quantitatively similar to those obtained

TABLE III. Best-fit parameters that define the radial basis functions  $F_k(R)=V(R, \theta_k)$ .

$\theta/^\circ$	$D/\text{cm}^{-1}$	$\alpha/\text{Å}^{-1}$	$R_p/\text{Å}$	$C_4/10^4$ $\text{cm}^{-1} \text{Å}^4$	$C_6/10^6$ $\text{cm}^{-1} \text{Å}^6$	$C_8/10^7$ $\text{cm}^{-1} \text{Å}^8$	$C_{10}/10^8$ $\text{cm}^{-1} \text{Å}^{10}$	$C_{12}/10^9$ $\text{cm}^{-1} \text{Å}^{12}$
0	2.9760	1.9325	5.2323	-1.5147	0.3117	0.5597	-3.4016	7.3867
10	8.6387	1.9035	4.9548	-3.2353	0.5924	0.8318	-1.3563	5.2783
20	9.9501	1.8594	4.9129	-2.9613	0.5607	-0.8681	-1.0078	3.8657
30	10.5736	1.8069	4.8539	-1.2428	0.3985	0.6007	-0.6038	2.0570
40	4.5695	1.7963	5.0584	-1.2185	0.2893	0.1337	-2.2009	3.7413
50	6.2186	1.7608	4.8354	-1.4606	0.3394	-0.4389	-0.5193	1.5109
60	12.2165	1.8456	4.3601	-1.1043	0.2348	0.1352	-1.5942	1.4833
70	6.2213	1.7502	4.4121	-0.1236	0.1819	-0.1332	-0.1657	0.2959
80	10.2655	1.7549	4.0053	0.1978	0.1448	-0.0874	-0.0844	0.0909
90	12.3285	1.7788	3.8349	0.3605	0.1325	-0.0692	-0.0663	0.0589

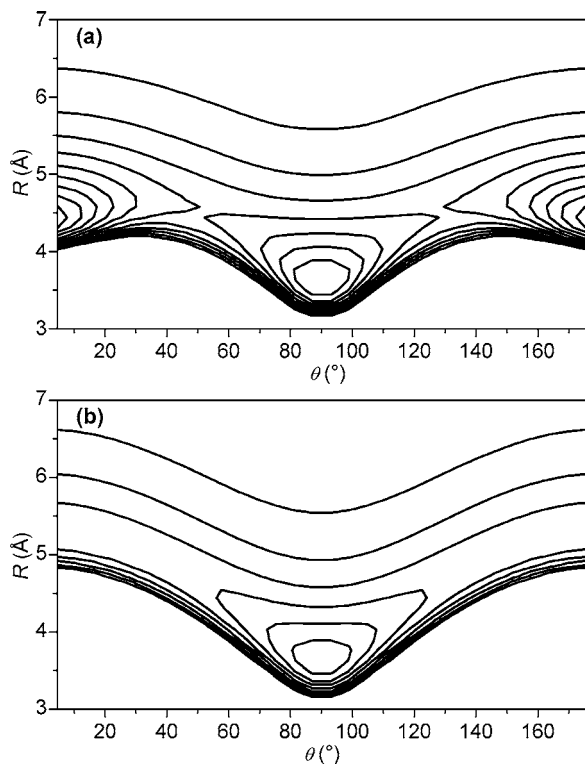


FIG. 1. The (a) He+Br $_2(X, v''=0)$  and (b) He+Br $_2(B, v''=12)$  potential-energy surfaces calculated as described in the text. The contours begin at  $-5$  cm $^{-1}$  and incrementally decrease by  $5$  cm $^{-1}$  in each panel.

from the DIM surface. While both surfaces provide energies that are in good agreement with experiment, we find that the agreement between the experimental binding energies is slightly better for the DIM surface. Other properties that are more sensitive to details of the potential will be needed to distinguish between these two surfaces.

For the remainder of the paper we will use the DIM surface. This choice is made based on the slightly better agreement between the calculated and experimental binding energies obtained when we use this surface. The fact that the DIM surface provides slightly better agreement with the experimental binding energies may at first seem surprising.

Having calculated the energies and wave functions for all of the bound He $\cdots$ <sup>79</sup>Br $_2$  intermolecular vibrational levels within the *X* and *B* states, we evaluate the positions and intensities of all of the lines in the rovibronic spectrum for

TABLE IV. Energies, average values of internuclear distances, and uncertainty of the bound intermolecular levels within the He+Br $_2(X, v''=0)$  potential.

$n''$	$E_{n''}/\text{cm}^{-1a}$	$\langle R \rangle/\text{\AA}$	$\sqrt{\langle R^2 \rangle - \langle R \rangle^2}/\text{\AA}$
0	-16.46	4.86	0.43
1	-16.46	4.86	0.43
2	-15.81	4.12	0.47
3	-8.41	4.80	0.60
4	-7.34	5.03	0.61
5	-5.39	4.88	0.68
6	-3.12	9.57	1.56

<sup>a</sup>All energies are reported relative to He+Br $_2(X, v''=0)$  dissociation asymptote.

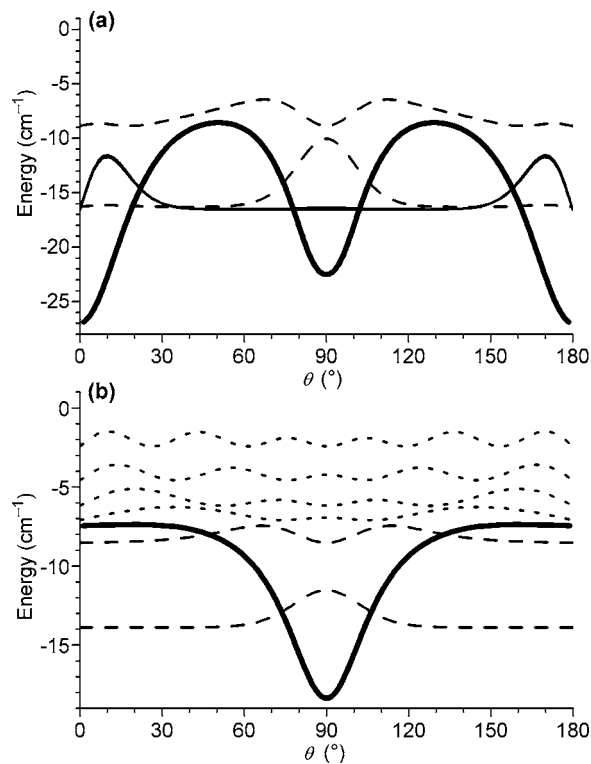


FIG. 2. The (a) He+<sup>79</sup>Br $_2(X, v''=0)$  and (b) He+<sup>79</sup>Br $_2(B, v''=12)$  adiabatic potentials, plotted as a function of angle about the Br $_2$  molecule,  $\theta$ , with  $\theta=0^\circ$  corresponding to the linear orientation. Superimposed on the potentials are the probability amplitudes of the lowest-energy intermolecular vibrational eigenstates. Each state is plotted so that zero amplitude corresponds to the energy of that level. To differentiate the three types of states, we plot those localized in the linear wells with solid lines, those localized in the *T*-shaped minimum with dashed lines, and the free rotor states are plotted with dotted lines. The calculations used to obtain these curves are described in the text.

temperatures ranging from 0.25 to 0.91 K, the temperature range over which the experimental LIF spectra were recorded. In order to investigate the dependence of the spectra on the intramolecular vibrational excitation of the Br $_2(B)$  moiety, He $\cdots$ <sup>79</sup>Br $_2$  spectra are calculated for the Br $_2$  *B*-*X*, 8-0, 12-0, and 21-0 regions, Figs. 3(a)–3(c), respectively. Temperatures of  $T=0.57$ , 0.58, and 0.51 K and Lorentzian line profiles with widths of 0.08, 0.10, and 0.30 cm $^{-1}$ , respectively, were used to best simulate the experimental data. The structures in these spectra are all qualitatively similar to each other and to the He $\cdots$ ICl spectra.<sup>9</sup> There is a well-resolved feature at  $\sim 2.5$  cm $^{-1}$  and a series of transitions in the broader feature that is peaked at  $\sim 10$  cm $^{-1}$  from the monomer band origin. As was observed for He $\cdots$ ICl, the lower-energy feature is associated with transitions from the ground-state level that is localized in the well on the *X*-state potential at  $90^\circ$  to the lowest-energy state on the *B*-state potential. The broader feature at higher energy reflects transitions from all three of the lowest-energy levels on the *X* state,  $n''=0-2$ , to excited intermolecular vibrational levels on the *B* surface,  $n' \geq 1$ . The lines attributed to transitions from the linear  $n''=0$  and 1 levels that appear within the higher-energy features tend to be more intense than those from the *T*-shaped,  $n''=2$  level, within the same feature, and

TABLE V. Theoretical and experimental energies, in  $\text{cm}^{-1}$ , of the bound intermolecular levels within the  $\text{He}+\text{Br}_2(B, \nu')$  potentials. All energies are reported relative to the  $\text{He}+\text{Br}_2(B, \nu')$  dissociation asymptote.

$n'$	$\nu'=8$		$\nu'=12$			$\nu'=21$
	DIM	Expt. <sup>a</sup>	DIM	<i>Ab initio</i> <sup>b</sup>	Expt. <sup>a</sup>	DIM
0	-13.52	-12.9	-13.42	-13.24	-12.7	-13.38
1	-8.08	-8.3	-7.94	-9.15	-8.1	-7.79
2	-7.05	-7.5	-6.90	-8.48	-7.3	-6.76
3	-6.10	-6.6	-5.95	-7.36	-6.4	-5.85
4	-4.73	-5.8	-4.64	-5.80	-5.6	-4.68
5	-2.60	...	-2.55	-1.57	-2.9	-2.71
6	-0.89	...	-0.89	-0.33	...	-1.20

<sup>a</sup>The uncertainty of the experimental energies is  $\pm 0.8 \text{ cm}^{-1}$  as dictated by the uncertainty of the binding energy of the linear  $\text{He}\cdots\text{Br}_2(X, \nu''=0)$  complex.

<sup>b</sup>The *ab initio* potential was evaluated with  $r$  fixed at the  $\text{Br}_2(B)$  equilibrium value,  $r=2.6776 \text{ \AA}$  (Ref. 20), and the energies were obtained using the rotational constant for  $^{79}\text{Br}_2(B, \nu'=12)$ .

we accordingly will refer to this feature as the linear feature. This observation is in accord with previously reported results of Buchachenko *et al.*<sup>14</sup>

### C. Experimental $\text{He}\cdots\text{Br}_2$ excitation spectra

The experimental LIF spectra of  $\text{He}\cdots^{79}\text{Br}_2$  were recorded in the  $\text{Br}_2 B-X$ , 8-0, 12-0 and 21-0 regions, and are shown in Figs. 3(d)–3(f), respectively. The spectra were recorded using identical expansion conditions, such that the monomer rotational temperature was measured to be  $\sim 0.5 \text{ K}$  in each. The spectra are plotted as a function of transition energy relative to the corresponding  $^{79}\text{Br}_2 B-X$ , 8-0, 12-0, and 21-0 band origins at 17 040.78, 17 561.14, and 18 497.66  $\text{cm}^{-1}$ , respectively.<sup>26</sup>

The feature observed at  $\sim 4 \text{ cm}^{-1}$  to higher energy than each of the  $^{79}\text{Br}_2 B-X$ ,  $\nu'-0$  band origins is attributed to rovibronic transitions of the  $\text{He}\cdots^{79}\text{Br}_2(X, \nu''=0)$  *T*-shaped conformer.<sup>13</sup> The broad feature centered at  $\sim 10 \text{ cm}^{-1}$  from the band origin has been previously attributed to overlapping transitions of the *T*-shaped and linear  $\text{He}\cdots^{79}\text{Br}_2(X, \nu''=0)$  complexes.<sup>14,16</sup> There is a slight shift of the *T*-shaped and

linear  $\text{He}\cdots^{79,79}\text{Br}_2$  features to higher transition energies with increasing  $\nu'$ , which is indicative of a slight decrease in the excited-state binding energy with  $\nu'$ . Based on the energy shift rule,<sup>27</sup> the small feature at  $\sim 8 \text{ cm}^{-1}$ , which is most easily observed in the 12-0 spectrum, is attributed to transitions of the higher-order  $\text{He}_2\cdots^{79}\text{Br}_2(X, \nu''=0)$  complex with the two He atoms localized near the plane that bisects the Br–Br bond. There is also a structureless continuum fluorescence signal observed throughout all of the  $\text{Br}_2 B-X$ ,  $\nu'-0$  regions investigated that has not been reported previously. The intensity of the background signal relative to the intensity of the  $\text{He}\cdots^{79}\text{Br}_2$  features is significantly larger in the 21-0 region compared to that observed in the 12-0 and 8-0 regions. It is important to note that in all cases, the intensity of the continuum signals track with the intensities of the higher-energy linear features as the expansion conditions are varied.

A number of weaker lines observed in the lower-energy regions of the spectra are presumably due to transitions of the  $\text{He}\cdots^{79,81}\text{Br}_2(X, \nu''=0)$  mixed isotopomers. Multiple action spectra were recorded in the  $\text{Br}_2 B-X$ , 12-0 region to

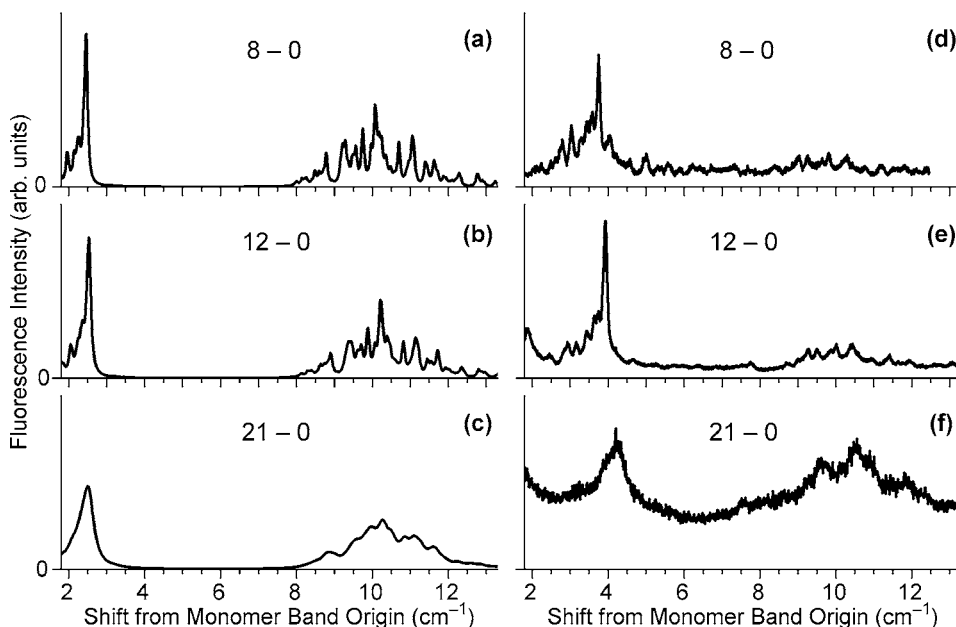


FIG. 3. The calculated, (a), (b), (c), and experimental, (d), (e), (f), spectra for  $\text{He}\cdots^{79}\text{Br}_2$  in the  $\text{Br}_2 B-X$ , 8-0, 12-0 and 21-0 regions plotted as functions of energy relative to the corresponding band origins at 17 040.78, 17 561.14, and 18 497.66  $\text{cm}^{-1}$ , respectively. The spectra were recorded at  $Z=x/d=21.2$  and with  $P_0=28.6 \text{ bar}$ , and the  $\text{Br}_2(X, \nu''=0)$  rotational temperatures were measured to be 0.57, 0.58, and 0.51 K for the three spectra. To facilitate comparison, these temperatures were also used in the calculated spectra.

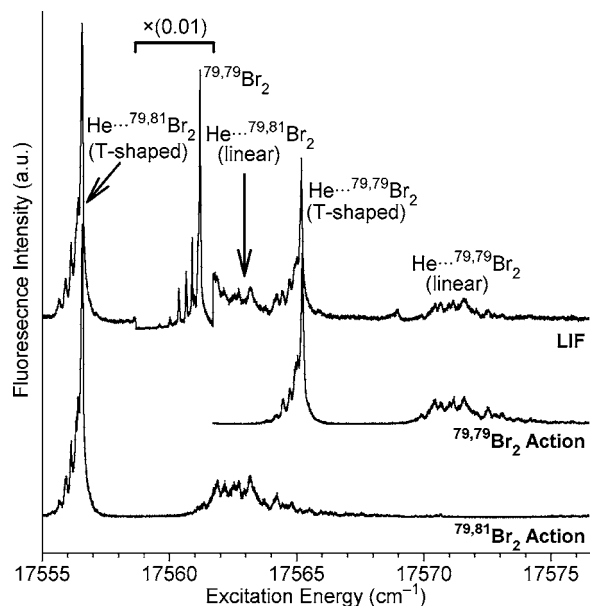


FIG. 4. Laser-induced fluorescence (LIF) and action spectra recorded in the Br<sub>2</sub> B-X, 12-0 spectral region using  $P_0=28.6$  bar and  $T_0=294.2$  K, and at a downstream distance  $Z=x/d=21.2$ . The intensity scale across the  $^{79,79}\text{Br}_2$  monomer band near  $17561\text{ cm}^{-1}$  is decreased by 100 times. The  $^{79,79}\text{Br}_2$  and  $^{79,81}\text{Br}_2$  action spectra were acquired with the probe laser fixed on the R-band heads of the  $^{79,79}\text{Br}_2$  and  $^{79,81}\text{Br}_2$  E-B, 1–11 transitions. All He...Br<sub>2</sub> features are labeled with the ground-state conformer associated with transitions within that feature.

definitively identify those features observed in the LIF spectra that can be associated with transitions of the He... $^{79,79}\text{Br}_2$  and He... $^{79,81}\text{Br}_2$  complexes. These spectra were recorded at several downstream distances by scanning the excitation laser through the Br<sub>2</sub> B-X, 12-0 spectral region with the probe laser fixed on the R-band head of either the  $^{79,79}\text{Br}_2$  or  $^{79,81}\text{Br}_2$  E-B, 1–11 transitions. The LIF, and  $^{79,79}\text{Br}_2$  and  $^{79,81}\text{Br}_2$  action spectra recorded at  $Z=x/d=21.2$  are shown in Fig. 4 offset from each other from top to bottom, respectively. The action spectrum obtained with the probe fixed on the  $^{79,79}\text{Br}_2$  E-B, 1–11 transition is dominated by the He... $^{79,79}\text{Br}_2$  T-shaped band and the broad He... $^{79,79}\text{Br}_2$  feature at  $17571\text{ cm}^{-1}$ . Comparison of this action spectrum with the LIF spectrum indicates that the same peaks within the higher-energy feature are observed in both spectra, thereby ruling out the possibility of contributions to this feature from rovibronic transitions of higher-order He... $^{79}\text{Br}_2(X, \nu''=0)$  clusters or from other isotopomers. Furthermore, the intensity of the higher-energy feature relative to that of the T-shaped feature observed in the action spectra track with those in the LIF spectra as the experimental conditions is varied. The action spectrum obtained by monitoring the  $^{79,81}\text{Br}_2$  E-B, 1–11 R-band head contains features at  $\sim 17556.5$  and  $17562.5\text{ cm}^{-1}$ , and appear very similar to the features associated with the transitions of the He... $^{79,79}\text{Br}_2(X, \nu''=0)$  complex.

More careful scrutiny of the LIF and action spectra recorded in the different spectral regions (Fig. 3) indicates that despite modest spectral congestion, there is a qualitative agreement between the number of lines, as well as their relative intensities, that are observed in the linear He... $^{79}\text{Br}_2$  features present in the 8-0 and 12-0 spectra. The linewidths

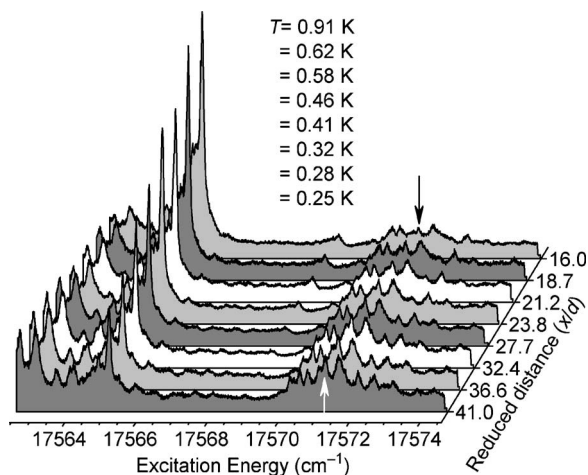


FIG. 5. Laser-induced fluorescence spectra recorded in the Br<sub>2</sub> B-X, 12-0 spectral region using the same source conditions,  $P_0=28.6$  bar and  $T_0=294.2$  K, and at eight different distances downstream from the nozzle orifice,  $x/d$ , where the diameter of the nozzle,  $d$ , is 1.0 mm. The  $^{79}\text{Br}_2(X, \nu''=0)$  rotational temperature associated with each spectrum is listed. Each spectrum has been normalized so that the total integrated intensity is unity. The arrows indicate the energy position that was used to track the intensity of the linear feature.

in the 12-0 region are only slightly broader than in the 8-0 region,  $\sim 0.10$  and  $\sim 0.08\text{ cm}^{-1}$ , respectively. Considering the  $0.06\text{-cm}^{-1}$  bandwidth of our excitation laser, these values are in fair agreement with the previously reported linewidths of the T-shaped features observed in each of the regions.<sup>13</sup> In contrast, the He... $^{79}\text{Br}_2$  features in the Br<sub>2</sub> B-X, 21-0 spectrum are significantly broadened and, as a result, do not exhibit the resolvable rotational structure observed in the other two regions. A trend of increased linewidths with increasing Br<sub>2</sub>(B,  $\nu'$ ) vibrational excitation was noted in previous spectroscopic studies of He...Br<sub>2</sub> (Refs. 13 and 28) and Ne...Br<sub>2</sub> (Ref. 29) complexes and was interpreted to be a result of rapid vibrational predissociation in the higher vibrational levels ( $\nu' > 18$ ).

The LIF spectra of the T-shaped and linear He... $^{79}\text{Br}_2(X, \nu''=0)$  complexes were recorded in the Br<sub>2</sub> B-X, 8-0, 12-0, and 21-0 spectral regions using the same source conditions,  $P_0=28.6$  bar and  $T_0=294.2$  K, and at eight different distances downstream from the nozzle orifice,  $Z=16.0, 18.7, 21.2, 23.8, 27.7, 32.4, 36.6$ , and  $40.7$ . The distance-dependent spectra recorded in the 12-0 region are shown in Fig. 5 with each spectrum normalized so that the total integrated intensity is unity. The rotational contour of the  $^{79}\text{Br}_2$  B-X,  $\nu''=0$  monomer feature recorded at each distance was fit to a Boltzmann distribution using the published  $^{79}\text{Br}_2$  X- and B-state spectroscopic constants.<sup>26</sup> For the 12-0 data, the monomer rotational temperature decreases monotonically from  $0.91(2)$  K at  $Z=16.0$  down to  $0.25(3)$  K at  $Z=40.7$ , as indicated in Fig. 5. In all of the spectral regions, the peak intensity of the T-shaped feature decreases and that of the linear feature increases monotonically with increasing  $Z$ , and thus decreasing  $T$ . It is particularly noteworthy that the ratios of the experimental intensities of the T-shaped to linear features,  $\text{Int}[T\text{-shaped}]/\text{Int}[\text{linear}]$ , observed in the 8-0 and 12-0 regions are nearly identical at each  $Z$  with values greater than 1 under all expansion conditions and down-

stream distances. For instance, this ratio is  $\sim 10$  in both spectra recorded at  $Z \approx 22$  and with a backing pressure of  $P_0 = 28.6$  bar. In contrast, this ratio decreases significantly for the spectra recorded in the 21-0 region, down to  $\sim 1$  under the same conditions. Despite the differences in the values of  $\text{Int}[T\text{-shaped}]/\text{Int}[\text{linear}]$ , the ratios decrease with approximately the same rate with increasing distance downstream in the expansion in all three spectral regions.

## V. COMPARISON OF EXPERIMENT AND THEORY

### A. Intensities

#### 1. Discrepancies between experimental and calculated intensities

The most notable difference between the experimental and calculated spectra for  $\text{He} \cdots {}^{79}\text{Br}_2$  is in the relative intensities of the two bands. For example, at 0.58 K, the  $T$ -shaped feature in the 12-0 experimental LIF spectrum is much more intense than the higher-energy, linear feature, Fig. 3. In contrast, the maxima in the intensities of the two features differ by less than a factor of 2 in the calculated spectrum. While small discrepancies between the experimental and theoretical spectra were reported for the  $\text{He} \cdots \text{ICl}$  system,<sup>9</sup> they were not as dramatic as found here. Since these two features are primarily attributed to transitions from the  $n''=2$  level for the lower energy,  $T$ -shaped feature, and the  $n''=0$  and 1 levels for the higher-energy, linear feature, changes in the binding energies of these states could have a large effect on the relative intensities of these bands. In fact, this spectrum is particularly sensitive to this energy difference because the three lowest-lying  $J''=0$  intermolecular vibrational states within the  $\text{He} + {}^{79}\text{Br}_2(X, \nu''=0)$  calculated PES differ in energy by only  $0.65 \text{ cm}^{-1}$ . To investigate the sensitivity of the relative intensities of the features,  $\text{Int}[T\text{-shaped}]/\text{Int}[\text{linear}]$ , on the relative binding energies, we shifted all of the states on the  $X$ -state potential that are localized in the  $T$ -shaped potential minimum by a constant wave-number shift  $\Delta E$  and recalculated the excitation spectrum. A plot of  $\text{Int}[T\text{-shaped}]/\text{Int}[\text{linear}]$  as a function of  $\Delta E$  is given in Fig. 6 for  $T=0.25, 0.58$ , and  $0.91$  K. As expected, there is a high sensitivity of the relative intensities to the relative binding energies of the three lowest intermolecular vibrational levels of the complex, and a shift of only  $-0.45 \text{ cm}^{-1}$  is sufficient to increase the intensity ratio by more than an order of magnitude at 0.25 K. Thus, the difference in the intensities of the experimental and theoretical features is partially attributable to a slight discrepancy in the relative binding energies of the two ground-state conformers.

What is also evident is that the relative peak intensities of the  $T$ -shaped and linear features in the  $\text{Br}_2 B-X$ , 21-0 region are nearly the same, whereas the peak intensity of the  $T$ -shaped feature is significantly larger than that of the linear feature in the 8-0 and 12-0 spectra. This difference is not attributed to varying Franck-Condon factors for the different  $\text{Br}_2 B-X, \nu''=0$  spectral regions, since the integrated intensities of the three bands are nearly the same in all three spectra. Calculations of spectra in these regions support this conclusion. Spectra with Lorentzian linewidths matching those measured experimentally,  $0.08, 0.10$ , and  $0.30 \text{ cm}^{-1}$ , were

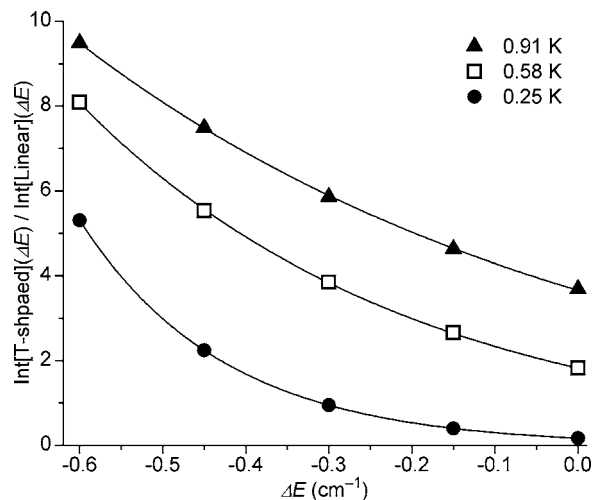


FIG. 6. The ratio of the calculated peak intensities of the  $T$ -shaped to linear features in the  $\text{Br}_2 B-X$ , 12-0 region, plotted as a function of the shift of the energies of the  $T$ -shaped levels relative to that of the linear levels,  $\Delta E$ , and using different temperatures;  $T=0.25$  K (black circles),  $T=0.58$  K (white squares), and  $T=0.91$  K (black triangles).

used in calculating the 8-0, 12-0, and 21-0 spectra, respectively. The relative peak intensities of the  $T$ -shaped and linear features in the calculated spectra do become comparable in the 21-0 region, following the experimental trend. Experiments performed in the time domain that can monitor the kinetics of the dissociation of these different intermolecular levels, similar to those performed on  $\text{Ne} \cdots \text{Br}_2(B, \nu')$  complexes,<sup>30</sup> could reveal insights into the fate of the excited-state molecules and perhaps the dynamics in the different intermolecular levels accessed by transitions of the  $T$ -shaped and linear conformers.

#### 2. The relative binding energies of the $T$ -shaped and linear $\text{He} \cdots {}^{79}\text{Br}_2(X, \nu''=0)$ conformers

Having demonstrated the sensitivity of the temperature dependence of the relative peak intensities to the relative binding energies of the two complexes, we turn our focus to analyzing the relative binding energies of the  $T$ -shaped and linear  $\text{He} \cdots {}^{79}\text{Br}_2(X, \nu''=0)$  conformers. The distance-dependent LIF spectra, Fig. 5, reveal that the intensities of nearly all of the lines within the broad feature at  $\sim 17571 \text{ cm}^{-1}$  increase with increasing  $Z$ , while the peak intensity of the  $T$ -shaped feature decreases monotonically with increasing distance. Using the ratio of the peak intensity of the  $T$ -shaped feature to that of the linear feature in the 12-0 LIF spectra and the monomer rotational temperatures measured at each of the eight distances, a thermodynamic model<sup>12</sup> was implemented to estimate the relative binding energies of the ground-state conformers. The model incorporates two major assumptions: the populations of the  $T$ -shaped and linear complexes,  $[T\text{-shaped}]$  and  $[\text{linear}]$ , are in a thermodynamic equilibrium characterized by the  ${}^{79}\text{Br}_2(X, \nu''=0)$  rotational temperature  $T$  and the peak intensities of the  $T$ -shaped and linear features observed in the LIF spectra are proportional to the ground-state populations of the conformers. A plot of the  $T$ -shaped to linear intensity ratios,  $\text{Int}[T\text{-shaped}]/\text{Int}[\text{linear}]$ , as a function of inverse tempera-

ture  $T^{-1}$  was fit to the ratio of the  $T$ -shaped to linear quantum mechanical partition functions in the high-temperature limit

$$\frac{\text{Int}[T\text{-shaped}](T)}{\text{Int}[Linear](T)} = aT^{1/2} \exp\left(\frac{-\Delta E}{k_B T}\right) \quad (8)$$

to estimate the relative ground-state binding energies of the conformers,  $\Delta E$ . Since only one intermolecular vibrational level is associated with the  $T$ -shaped conformer and that the two linear levels are nearly degenerate and we can thus treat it as a single level, the  $\Delta E$  value obtained from the fit is taken to represent the difference in the ground-state binding energies of the  $T$ -shaped and linear He...<sup>79</sup>Br<sub>2</sub>( $X, \nu''=0$ ) conformers.

The presence of the background continuum signal and the partial overlap of the linear He...<sup>79,81</sup>Br<sub>2</sub> feature with the He...<sup>79,79</sup>Br<sub>2</sub> features in each Br<sub>2</sub>  $B$ - $X, \nu''=0$  region precludes a direct measurement of the peak intensities of the  $T$ -shaped and linear features. Therefore, the maximum intensity at the band head, at 17 565.2 cm<sup>-1</sup>, less a contribution from the background signal, was selected to monitor the change in the intensity of the  $T$ -shaped He...<sup>79,79</sup>Br<sub>2</sub> feature. The contribution from the background was estimated using the average intensity over a small wave-number region around ~17 565.6 cm<sup>-1</sup>, slightly to the blue of the  $T$ -shaped band head. The intensity in this region was approximately constant in all of the normalized LIF spectra, and the intensity of the band head decreased monotonically with respect to this intensity.

Determining the intensity of the linear feature was a bit more involved since rovibrational lines attributable to transitions of both the  $T$ -shaped and linear conformers are believed to contribute to this feature. The theoretical calculations suggest that the lines at 17 571.1 and 17 571.5 cm<sup>-1</sup> are predominantly due to the transitions of the linear conformer. Given that the rate of change of the intensity of the line at 17 571.1 cm<sup>-1</sup>, indicated by the arrow in Fig. 5, with increasing distance relative to the intensity of the  $T$ -shaped band head was larger than the rate of change of the 17 571.5-cm<sup>-1</sup> line, the lower-energy line is presumed to have more linear contribution. Consequently, the intensity of the 17 571.1-cm<sup>-1</sup> feature was chosen to monitor the changes in the population of the linear He...<sup>79</sup>Br<sub>2</sub>( $X, \nu''=0$ ) conformer with changing distance and temperature. An estimate of the background signal intensity was subtracted off of the line intensity, with this estimate giving rise to the major error in the line intensities.

To partially verify the manner in which the peak intensities were obtained, action spectra were recorded at  $Z=21.2$  and  $27.7$  to quantitatively compare the values of  $\text{Int}[T\text{-shaped}](T)/\text{Int}[Linear](T)$  for He...<sup>79,79</sup>Br<sub>2</sub> observed without overlapping spectral features associated with the other isotopomers and without the presence of the continuum signal. The peak intensities of the  $T$ -shaped feature were obtained directly from the values at the band head maximum. Because of the overlapping  $T$ -shaped and linear lines in the linear feature, the linear peak height was determined following the same procedure used for the LIF spectra. The intensity ratios of 12.6(6) and 7.6(4) determined from the action

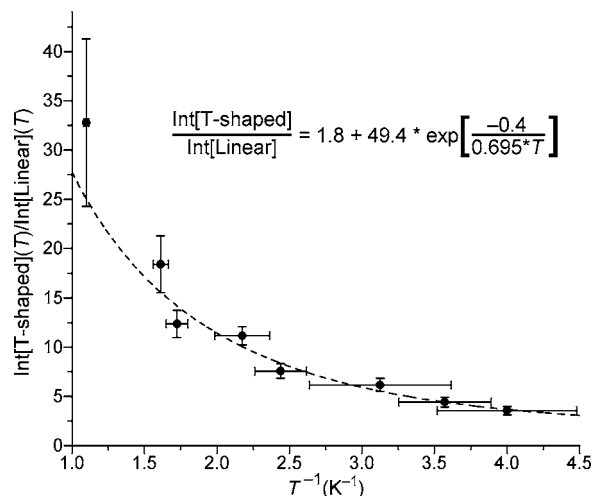


FIG. 7. The He...<sup>79</sup>Br<sub>2</sub> intensity ratios,  $\text{Int}[T\text{-shaped}](T)/\text{Int}[linear](T)$ , obtained from the 12-0 LIF spectra recorded at different distances, Fig. 4, plotted as a function of the inverse of the Br<sub>2</sub>( $X, \nu''=0$ ) rotational temperature  $T^{-1}$  measured at each distance. The dashed line represents a fit of the experimental data to Eq. (8) plus an offset, with best-fit values indicated in the included equation.

spectra at  $Z=21.2$  and  $26.8$ , respectively, are in excellent agreement with those obtained from the LIF spectra, 12.4(1.0) and 7.6(7).

The He...<sup>79</sup>Br<sub>2</sub> intensity ratios,  $\text{Int}[T\text{-shaped}](T)/\text{Int}[Linear](T)$ , obtained from the 12-0 LIF spectra in Fig. 5, are shown in Fig. 7, plotted as a function of the inverse of the Br<sub>2</sub>( $X, \nu''=0$ ) rotational temperature  $T^{-1}$ . An order of magnitude change in the relative populations is observed over these distances, indicating a significant shift in population to the linear conformer with cooling and that the linear conformer is more thermodynamically stable than the  $T$ -shaped conformer. A preliminary fit of the data using Eq. (8) indicated that an offset had to be included to get a quality fit, and this offset may be an indication of deficiencies in assuming that the populations are in thermodynamic equilibrium and in this model. Nevertheless, we used Eq. (8) plus an offset to fit the experimental data, dashed line in Fig. 7, and to obtain an estimate of  $\Delta E=0.4(2)$  cm<sup>-1</sup>. As a confirmation of this approach, we repeated the above analysis on the calculated spectra for the Br<sub>2</sub>  $B$ - $X, 12-0$  region and determined that the linear conformer is 0.5 cm<sup>-1</sup> more strongly bound than the  $T$ -shaped conformer, which is in fair agreement with a difference of 0.65 cm<sup>-1</sup> between the  $J''=0$  levels of each conformer, Table IV.

## B. Absolute binding energies of the $T$ -shaped and linear He...<sup>79</sup>Br<sub>2</sub>( $X, \nu''=0$ ) conformers

Having estimated the relative binding energies of the two conformers, we turn our attention to determining the absolute binding energies of the  $T$ -shaped and linear ground-state conformers. High-resolution (0.06 cm<sup>-1</sup>) He...<sup>79</sup>Br<sub>2</sub> action spectra were recorded in the Br<sub>2</sub>  $B$ - $X, 11-0$  region by monitoring the formation of the  $\Delta \nu'=0, \text{Br}_2(B, \nu'=11)$  dissociation product channel via the <sup>79</sup>Br<sub>2</sub>  $E$ - $B, 1-11$  transition. The spectrum is shown in Fig. 8, plotted as a function of energy from the <sup>79</sup>Br<sub>2</sub>  $B$ - $X, 11-0$  band origin, 17 436.9 cm<sup>-1</sup>.

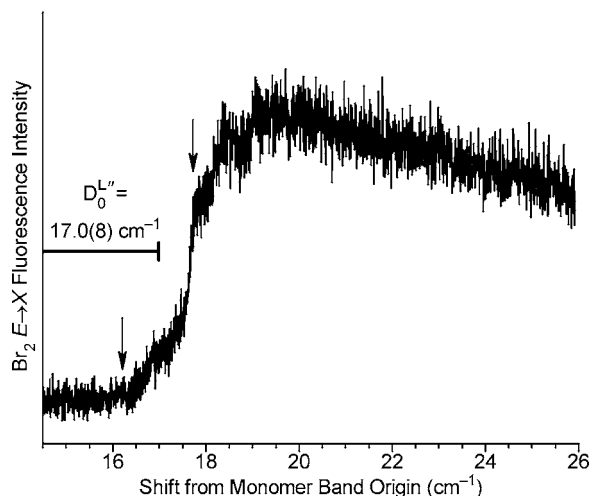


FIG. 8. A portion of the action spectrum recorded in the  $\text{Br}_2$   $B$ - $X$ , 11-0 region and with the probe laser fixed on the  $R$ -band head of the  $^{79}\text{Br}_2$   $B$ - $X$ , 1-11 transition. The spectrum is plotted as a function of energy from the  $^{79}\text{Br}_2$   $B$ - $X$ , 11-0 band origin, 17 436.9  $\text{cm}^{-1}$ . The turn-on is estimated to be 17.0  $\text{cm}^{-1}$  from the monomer band origin, indicating that the linear  $\text{He}\cdots^{79}\text{Br}_2(X, \nu''=0)$  complex is bound by that amount. The error in the turnon energy is bracketed between the regions indicated with the arrows,  $\pm 0.8 \text{ cm}^{-1}$ .

Although not shown in Fig. 8, the region immediately to higher energy than the  $^{79}\text{Br}_2$   $B$ - $X$ , 11-0 monomer band was featureless until the onset of the continuum signal  $\sim 17 \text{ cm}^{-1}$  to higher energy from the monomer band origin, as shown. The broad continuum fluorescence was found to extend at least 40  $\text{cm}^{-1}$  to even higher energy. The signals for this experiment were quite weak, and the somewhat acceptable signal-to-noise levels over the region shown in Fig. 8 required  $\sim 27 \text{ h}$  of total acquisition time. The intensity of the continuum signal was observed to track with the intensity of the linear feature and not the  $T$ -shaped feature as the expansion conditions and downstream distances at which the spectra were recorded were varied. Thus, as was observed for  $\text{He}\cdots\text{ICl}$ ,<sup>12,20</sup>  $\text{Ne}\cdots\text{ICl}$ ,<sup>31</sup> and  $\text{Ar}\cdots\text{I}_2$ ,<sup>22</sup> the continuum signal observed here is attributed to bound-free transitions of the linear  $\text{He}\cdots^{79}\text{Br}_2(X, \nu''=0)$  complex to the continuum of states lying just above the  $\text{He} + ^{79}\text{Br}_2(B, \nu'=11)$  dissociation limit.

By fixing the probe laser on the  $R$ -band head of the  $^{79}\text{Br}_2$   $E$ - $B$ , 1-11 transition, the energy difference between the  $^{79}\text{Br}_2$   $B$ - $X$ , 11-0 band origin and the continuum turn-on directly reveals the ground-state binding energy of the linear  $\text{He}\cdots^{79}\text{Br}_2(X, \nu''=0)$  conformer.<sup>12,20</sup> Similar action spectra for the  $\text{He}\cdots\text{I}^{35}\text{Cl}$  complex using the same 0.06- $\text{cm}^{-1}$  resolution revealed a highly structured continuum resulting from rotational predissociation of the  $\text{He}\cdots\text{I}^{35}\text{Cl}(X, \nu'=2)$  complex prepared in an intermolecular vibrational level that is energetically at the dissociation limit.<sup>12</sup> Subsequent two-laser pump-probe experiments performed by exciting at different regions and on the discrete lines along the turn-on region of the continuum signal identified the precise excitation energy that formed  $\text{I}^{35}\text{Cl}(B, \nu'=2, j')$  products with the least amount of rotational excitation,  $j'$ . This excitation energy was then taken to be the transition energy of the ground-state linear complex that just accesses the  $\text{He} + \text{I}^{35}\text{Cl}(B, \nu'=2, j'=0)$

asymptote.<sup>21</sup> There is no discernable structure in the  $\text{He}\cdots^{79}\text{Br}_2$  turn-on region of the continuum signal suggesting that there is not an accidental resonance of a  $\text{He}\cdots^{79}\text{Br}_2(B, \nu'=11)$  intermolecular vibrational level with the asymptotic region of the  $\text{He} + ^{79}\text{Br}_2(B, \nu'=11)$  potential. Furthermore, the  $^{79}\text{Br}_2(B, \nu'=11, j')$  product state distribution is extremely cold, with approximately the same distribution observed when exciting between 17.0 and 17.8  $\text{cm}^{-1}$  in the turn-on region. Therefore, the turn-on of the continuum and thus the ground-state binding energy was approximated with errors that included the breadth in energy associated with the rotational Boltzmann distribution of the linear  $\text{He}\cdots^{79}\text{Br}_2(X, \nu''=0)$ .

Referring to Fig. 8, the continuum signal begins to “turn on”  $\sim 16.2 \text{ cm}^{-1}$  to higher energy from the monomer band origin, which is indicated by the arrow on the left of figure. The intensity of the continuum gradually increases until  $\sim 17.7 \text{ cm}^{-1}$  at which point there is a discrete rise within a 0.1- $\text{cm}^{-1}$  increment, marked by the arrow to the right. We take the midpoint of this energy region to be the excitation energy that accesses the dissociation limit, indicating a ground-state binding energy of 17.0  $\text{cm}^{-1}$  for the linear conformer and the breadth of this region  $\pm 0.8 \text{ cm}^{-1}$ , to be the error. The ground-state binding energy of the linear  $\text{He}\cdots^{79}\text{Br}_2(X, \nu''=0)$  conformer, 17.0(8)  $\text{cm}^{-1}$ , and our experimentally determined binding energy difference, 0.4(2)  $\text{cm}^{-1}$ , reveal a  $\text{He}\cdots^{79,79}\text{Br}_2(X, \nu''=0)$   $T$ -shaped binding energy of 16.6(8)  $\text{cm}^{-1}$ . These binding energies are slightly larger than the values reported in Table IV, 16.46 and 15.81  $\text{cm}^{-1}$ , calculated using our *ab initio* surface. A value of 16.6(8)  $\text{cm}^{-1}$  for the binding energy of the ground-state  $T$ -shaped conformer, however, does agree extremely well with the value reported previously by Jahn *et al.*,<sup>33</sup> 17.0(1.5)  $\text{cm}^{-1}$ .

### C. Determination of the binding energies on the $B$ -state surface

Having determined the binding energies of the two conformers on the  $X$ -state potential, we turn our attention to ascertaining the relative binding energies of the intermolecular vibrational levels on the  $B$ -state potential. The  $n'=0$  state is the easiest of these to obtain from the experimental spectrum since the low-energy feature results from transitions of the  $T$ -shaped complex to this level. The  $\sim 3.9\text{-cm}^{-1}$  spectral shift of the  $T$ -shaped band origin from the monomer band origin in the 12-0 region and the 16.6(8)- $\text{cm}^{-1}$  binding energy for the  $\text{He}\cdots^{79,79}\text{Br}_2(X, \nu''=0)$   $T$ -shaped conformer indicate an excited-state binding energy of  $\sim 12.7 \text{ cm}^{-1}$  for the lowest intermolecular vibrational level in the  $\text{He} + ^{79}\text{Br}_2(B, \nu'=12)$  potential with an equilibrium  $T$ -shaped geometry. In a similar manner, a binding energy of  $\sim 12.9 \text{ cm}^{-1}$  was estimated for the  $n'=0$  level within the  $\text{He} + ^{79}\text{Br}_2(B, \nu'=8)$  potential. These binding energies also agree quite well with those reported previously, a value of 13.5(1.0)  $\text{cm}^{-1}$  was reported for the binding energy of the  $n'=0$  level within the  $\text{He} + ^{79}\text{Br}_2(B, \nu'=44)$  PES.<sup>33</sup>

To obtain experimental energies of higher-lying intermolecular vibrational levels within the  $B$ -state potentials, we

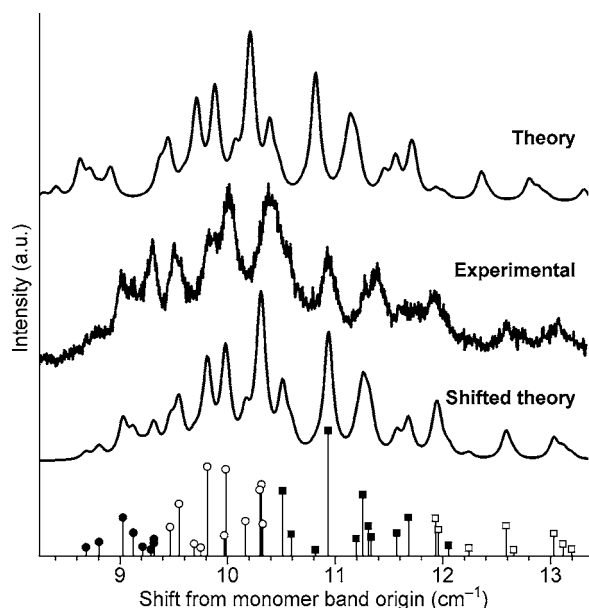


FIG. 9. Expanded views of the theoretical and experimental spectra in the Br<sub>2</sub> B-X, 12-0 region spanning the linear feature and plotted as a function of energy from the monomer band origin, 17 561.14 cm<sup>-1</sup>. The top plot is the theoretical spectrum obtained by including all rotational lines from ground-state levels with  $J'' \leq 2$  and relative populations associated with a rotational temperature of 0.28 K. A Lorentzian linewidth of 0.10 cm<sup>-1</sup> was also utilized to best simulate the experimental spectra. The second plot is the experimental spectrum recorded using a backing pressure of  $P_0=28.6$  bar and recorded at a downstream distance of  $Z=x/d=41$ , for which a rotational temperature of 0.28 K was measured. The third plot is the calculated spectrum obtained by shifting around the band origins of the transitions accessing the different  $n'$  intermolecular vibrational levels to achieve the best agreement with the experimental spectrum. The stick spectra for the shifted spectrum have symbols to indicate those lines that access common excited state intermolecular vibrational levels:  $n'=1$  (black circles);  $n'=2$  (open circles);  $n'=3$  (black squares);  $n'=4$  (open squares).

first utilized the theoretical spectra obtained using the DIM potential to assist in making assignments of the lines observed within the linear features observed in the Br<sub>2</sub> B-X, 8-0, and 12-0 spectral regions. Since the experimental spectra are quite cold, only those transitions from the  $J''=0, 1$ , and 2 rotational levels of the ground-state linear conformer were included in the calculated spectra, and the experimental rotational temperature of 0.28 K was used. Rotational linewidths of 0.08 and 0.10 cm<sup>-1</sup> were used to best represent the experimentally observed linewidths for the spectra in the 8-0 and 12-0 regions, respectively. The calculated and experimental spectra for the 12-0 region are shown as the top two traces in Fig. 9. While there is qualitative agreement in the breadth and overall shape of this feature in the two spectra, assignments on a line-by-line basis cannot be made. We therefore chose to use the calculations as a guide and adjust the band origins of the different calculated intermolecular vibrational bands to try and optimize the agreement. In this way, the rotational structure associated with each band is maintained, but the overall contour of the linear feature can change significantly as the overlap in the rotational structure of the different vibrational bands is changed. Significantly better agreement between the experimental spectrum and the shifted calculated spectrum, second and third plots in Fig. 9, was obtained with only slight shifts in the vibrational band

origins. As an indicator of the composition of the structure observed within the band, we have included the stick spectrum associated with the optimized calculated spectrum, with those rotational lines accessing the same excited-state intermolecular vibrational level labeled with a common symbol. The shifted band origins were then used with the binding energy of the ground-state linear conformer, 17.0(8) cm<sup>-1</sup>, to obtain the experimental binding energies of the intermolecular levels with  $n' \geq 1$ .

The experimental excited-state binding energies and those calculated using the DIM PES are reported in Table V. Since there was significant line broadening in the experimental spectrum recorded in the Br<sub>2</sub> B-X, 21-0 region, binding energy assignments could not be made for the He + Br<sub>2</sub>(B,  $\nu'=21$ ) PES, but the calculated values are still included for comparison. As expected, with increasing Br<sub>2</sub>(B,  $\nu'$ ) vibrational excitation, the intermolecular levels become slightly less strongly bound. The energies obtained using the *ab initio* He + Br<sub>2</sub>(B) PES are included for comparison. In this case, we used a slice through the *ab initio* surface that was computed for a fixed Br-Br distance of 2.6776 Å,<sup>18</sup> and we used the rotational constant for Br<sub>2</sub>(B,  $\nu'=12$ ). The agreement with the experimental values appears to be slightly better for the DIM model, rather than the PES obtained using the *ab initio* points.

At first, this result may seem surprising, that a semi-empirical DIM surface obtained by adiabatically averaging the full three-dimensional potential over a specific vibrational state of the system should provide a better description of the intermolecular vibrational structure than a purely *ab initio* surface. We attribute this to a number of factors. First, the reported two-dimensional *ab initio* surface was obtained at a single Br-Br distance and for a relatively small number of angles. Work on the analogous ground-state potential, described above, showed that the angular cuts reported in Ref. 18 were not sufficient to fully sample the anisotropy of the potential especially near the linear configuration. In addition, as in previous work on He...ICl (Ref. 21) and Ne...OH (Ref. 32) excited-state potentials, we find that by scaling the He + Br<sub>2</sub>(B,  $\nu'=12$ ) *ab initio* surface by an overall scaling factor of 0.9, we can bring the mean absolute difference between the experimental and calculated energies to 2.58 cm<sup>-1</sup>, comparable agreement to what is achieved for the DIM surface (1.51 cm<sup>-1</sup>). Furthermore, recent work by us on He...ICl (Ref. 12) showed that even a relatively simple model for the excited-state potential surface can accurately reproduce the experimental binding energies. This is because most of the states that are probed experimentally lie above the barrier to free rotation on this surface, as shown in Fig. 2(b). As such, if the energy difference between the T-shaped minimum and the linear saddle point as well as the curvature of the T-shaped minimum are correct the experimental binding energies can be reproduced quite accurately even with a fairly simplistic model of the potential surface. The above comments indicate a rather low sensitivity of the vibrational structure on the B state of these He-dihalogen complexes on the potential surface rather than specific problems with the previously reported potential surfaces for these complexes.

## VI. CONCLUSIONS

A combined experimental and theoretical approach has been used to present evidence of the existence of a linear  $\text{He}\cdots\text{Br}_2(X, \nu''=0)$  conformer. Our theoretical calculations reveal an appreciable effective barrier of  $\sim 10\text{ cm}^{-1}$  separating the two lowest intermolecular levels of the  $\text{He}\cdots^{79}\text{Br}_2(X, \nu''=0)$  complex,  $n''=0$  and  $n''=1$ , corresponding to the linear conformer, and the next higher level,  $n''=2$ , which has a rigid  $T$ -shaped geometry. The probability amplitudes of the  $T$ -shaped and linear conformers are highly localized within each well; only  $\sim 1\%$  of the  $T$ -shaped (linear) probability amplitude is found in the linear ( $T$ -shaped) well. These theoretical results suggest that the  $T$ -shaped and linear  $\text{He}\cdots^{79}\text{Br}_2(X, \nu''=0)$  complexes can be regarded as distinct stereoisomers.

The changing intensities of the two features observed in the  $\text{He}\cdots^{79}\text{Br}_2$  rovibronic spectra with decreasing temperature in a supersonic expansion indicate that these features are indeed associated with two distinct conformers,  $T$ -shaped and linear, and this is corroborated by comparisons with the calculated spectrum. These intensity variations show that it is possible to stabilize different conformers of a Rg-homonuclear complex, and that the linear  $\text{He}\cdots\text{Br}_2(X, \nu''=0)$  conformer is more thermodynamically stable than the  $T$ -shaped conformer. The linear and  $T$ -shaped binding energies determined experimentally,  $17.0(8)$  and  $16.6(8)\text{ cm}^{-1}$ , agree fairly well with our calculated values,  $16.5$  and  $15.8\text{ cm}^{-1}$ , respectively. These results are significant because both the theory and experiment were able to resolve the small energy difference between the conformers, and both got the correct ordering, i.e., the linear  $\text{He}\cdots^{79}\text{Br}_2(X, \nu''=0)$  conformer is more strongly bound than the  $T$ -shaped conformer. From an experimental point of view, the results are quite remarkable given the simplicity of the approach. The capacity of the thermodynamic model to resolve the binding energy difference between the nearly isoenergetic  $\text{He}\cdots^{79}\text{Br}_2(X, \nu''=0)$  conformers and achieve such good agreement with the theoretical results is quite promising. The experimental methodology presented in this manuscript may prove to be a valuable tool in the characterization of the ground-state intermolecular potentials of other weakly bound complexes.

## ACKNOWLEDGMENTS

One of the authors (A.B.M.) gratefully acknowledges support from the National Science Foundation under Grant Nos. CHE-0200968/CHE-0515627. Another author (R.A.L.) is indebted to the David and Lucile Packard Foundation for a Fellowship in Science and Engineering and to the National Science Foundation for a CAREER Award, CHE-0346745 for supporting these research efforts.

- <sup>1</sup>D. H. Levy, *Adv. Chem. Phys.* **47**, 323 (1981).
- <sup>2</sup>A. Rohrbacher, N. Halberstadt, and K. C. Janda, *Annu. Rev. Phys. Chem.* **51**, 405 (2000).
- <sup>3</sup>A. Rohrbacher, J. Williams, and K. C. Janda, *Phys. Chem. Chem. Phys.* **1**, 5263 (1999).
- <sup>4</sup>S. J. Harris, S. E. Novick, and W. Klemperer, *J. Chem. Phys.* **61**, 193 (1974).
- <sup>5</sup>S. E. Novick, S. J. Harris, K. C. Janda, and W. Klemperer, *Can. J. Phys.* **53**, 2007 (1975).
- <sup>6</sup>K. Higgins, F.-M. Tao, and W. Klemperer, *J. Chem. Phys.* **109**, 3048 (1998).
- <sup>7</sup>J. B. Davey, A. C. Legon, and E. R. Waclawik, *Chem. Phys. Lett.* **306**, 133 (1999).
- <sup>8</sup>M. D. Bradke and R. A. Loomis, *J. Chem. Phys.* **118**, 7233 (2003).
- <sup>9</sup>A. B. McCoy, J. P. Darr, D. S. Boucher, P. R. Winter, M. D. Bradke, and R. A. Loomis, *J. Chem. Phys.* **120**, 2677 (2004).
- <sup>10</sup>R. Prosimiti, C. Cunha, P. Villarreal, and G. Delgado-Barrio, *J. Chem. Phys.* **117**, 7017 (2002).
- <sup>11</sup>D. S. Boucher, M. D. Bradke, J. P. Darr, and R. A. Loomis, *J. Phys. Chem. A* **107**, 6901 (2003).
- <sup>12</sup>D. S. Boucher, J. P. Darr, M. D. Bradke, R. A. Loomis, and A. B. McCoy, *Phys. Chem. Chem. Phys.* **6**, 5275 (2004).
- <sup>13</sup>D. G. Jahn, W. S. Barney, J. Cabalo, S. G. Clement, A. Rohrbacher, T. J. Slotterback, J. Williams, and K. C. Janda, *J. Chem. Phys.* **104**, 3501 (1996).
- <sup>14</sup>A. A. Buchachenko, R. Prosimiti, C. Cunha, G. Delgado-Barrio, and P. Villarreal, *J. Chem. Phys.* **117**, 6117 (2002).
- <sup>15</sup>A. Valdés, R. Prosimiti, P. Villarreal, and G. Delgado-Barrio, *Mol. Phys.* **102**, 2277 (2004).
- <sup>16</sup>M. I. Hernández, T. González-Lezana, G. Delgado-Barrio, P. Villarreal, and A. A. Buchachenko, *J. Chem. Phys.* **113**, 4620 (2000).
- <sup>17</sup>R. Prosimiti, C. Cunha, P. Villarreal, and G. Delgado-Barrio, *J. Chem. Phys.* **116**, 9249 (2002).
- <sup>18</sup>M. P. de Lara-Castells, A. A. Buchachenko, G. Delgado-Barrio, and P. Villarreal, *J. Chem. Phys.* **120**, 2182 (2004).
- <sup>19</sup>J. M. Skene and M. I. Lester, *Chem. Phys. Lett.* **116**, 93 (1985).
- <sup>20</sup>J. P. Darr, A. C. Crowther, and R. A. Loomis, *Chem. Phys. Lett.* **378**, 359 (2003).
- <sup>21</sup>J. P. Darr, R. A. Loomis, and A. B. McCoy, *J. Chem. Phys.* **122**, 044318 (2005).
- <sup>22</sup>J. P. Darr, J. J. Glennon, and R. A. Loomis, *J. Chem. Phys.* **122**, 131101 (2005).
- <sup>23</sup>M. J. Frisch, G. W. Trucks, H. B. Schlegel *et al.*, GAUSSIAN98 (Revision A.10), (Gaussian, Inc., Pittsburgh PA, 2001).
- <sup>24</sup>A. Bergner, M. Dolg, W. Kuechle, H. Stoll, and H. Preuss, *Mol. Phys.* **80**, 1431 (1993).
- <sup>25</sup>S. M. Cybulski and R. R. Toczyłowski, *J. Chem. Phys.* **111**, 10520 (1999).
- <sup>26</sup>R. F. Barrow, T. C. Clark, J. A. Coxon, and K. K. Yee, *J. Mol. Spectrosc.* **51**, 428 (1974).
- <sup>27</sup>J. E. Kenny, K. E. Johnson, W. Sharfin, and D. H. Levy, *J. Chem. Phys.* **72**, 1109 (1980).
- <sup>28</sup>L. J. van de Burgt, J.-P. Nicolai, and M. C. Heaven, *J. Chem. Phys.* **81**, 5514 (1984).
- <sup>29</sup>B. A. Swartz, D. E. Brinza, C. M. Western, and K. C. Janda, *J. Phys. Chem.* **88**, 6272 (1984).
- <sup>30</sup>J. A. Cabrera, C. R. Bieler, B. C. Olbricht, W. E. van der Veer, and K. C. Janda, *J. Chem. Phys.* **123**, 054311 (2005).
- <sup>31</sup>D. B. Strasfeld, J. P. Darr, and R. A. Loomis, *Chem. Phys. Lett.* **397**, 116 (2004).
- <sup>32</sup>H.-S. Lee, A. B. McCoy, R. R. Toczyłowski, and S. M. Cybulski, *J. Chem. Phys.* **113**, 5736 (2000).
- <sup>33</sup>D. G. Jahn, S. G. Clement, and K. C. Janda, *J. Chem. Phys.* **101**, 283 (1994).